A New Investigation into Al-Cu Dissimilar Joint by SiC Nanoparticle during the FSSW Process: Influence of Rotational Speed and Dwell Time

Mehdi Alizadeh
Behrouz Bagheri (b.bagheri@aut.ac.ir)
Amirkabir University of Technology
Ali Shamsipur
Amin Abdollahzadeh
Seyyed Ehsan Mirsalehi

Research Article

Keywords: Friction stir spot welding, SiC nanoparticle, Microstructure, Intermetallic compounds (IMCs), Mechanical behaviors

Posted Date: May 17th, 2022

DOI: https://doi.org/10.21203/rs.3.rs-1640449/v1

Abstract

Friction stir spot welding (FSSW) was implemented to joining of AA2024-T4 and commercially pure copper with SiC nanoparticles as a reinforcing particle for the first time. The influence of welding parameters namely rotational speed (1300, 1600, and 1900 rpm) and dwell time (2, 4, and 6 s) on microstructure and mechanical characteristics of the welds were studied. For this purpose, macro-and microstructures, shear tensile strength, and microhardness of the joints were investigated. The grain size of the stir zone on copper and aluminum sides decreases from 45.1 to 10.5 μm and 62.2 to 14.5 μm as rotational speed and dwell time decrease. Furthermore, the size of the weld zone increased as rotational speed and dwell time increased. The results revealed the formation of AlCu and Al_2Cu intermetallic compounds in the weld zone. The thickness of the IMCs layer in the interface joint increases as input heat increases. It was found that there is a direct relationship between the shear strength of weld specimens and rotational speed and dwell time during the FSSW process. The microhardness value of the joint zone was significantly improved from HV 122 to HV 156 with an increase in rotational speed and dwell time.

1. Introduction

The joining of dissimilar materials has been investigated as a prominent engineering strategy that causes a number of benefits including lightweight, hybrid properties, cost savings, structures, improved performance, and more [1–3]. Copper (Cu) and aluminum (Al) welding is considered a dissimilar combination that is applied for appealing utilization in various industries, such as aerospace and electronic components, e-mobility in automotive, electric wires, and mechanical components [4]. The joining of Al-Cu owing to the various characteristics (chemical and physical properties) of these two materials has been challenging for researchers using conventional fusion welding technologies. [5]. The creation of various defects such as porosity, solidification cracking, poor appearance as well as the formation of some harmful intermetallic compounds (IMCs) layers is common during the fusion joining techniques [6, 7]. To address the joining of difficult-to-melt structural materials such as Cu and Al alloys, friction stir welding (FSW) is known as an effective method among engineers because of its solid-state nature [8–10]. In order to achieve the stirring-mixing mechanism during the FSW-based method, a non-consumable or rigid tool is used where the material flow is influenced by the tool's geometry and the welding temperature of the weldment materials [11–13]. Cao et al. [14] investigated the impact of post welding heat treatment on microstructure evolution and mechanical performance of the FSW-ed Al-Cu joint. They indicated that the intermetallic compounds layer played a fundamental role in the metallurgical bonding such as final joint strength and hardness. The role of pin geometry and joining parameters during the FSW of Al-Cu dissimilar joining was studied by Muthu and Jayabalan [15]. It was found that the plain taper pin profile shows the stir zone with refined grains and maximum mechanical properties compared to other used tool pins. Akinlabi et al. [16] analyzed the friction stir welding of Al-Cu dissimilar joint under different rotational and feed rate speeds. They found that welding with a rotational speed of 950 r/min and a transfer speed of 300 mm/min presents the lowest corrosion rate. Friction stir spot welding of Al-Cu alloys with single and multi-spots was examined by Garg and Bhattacharya [17]. They found that the formation of the intermetallic compound near the joint interface provides the maximum thickness and failure occurs in the welding interface.

Recently, the introduction of nano-particle reinforcing such as metals and ceramics namely SiC, Al_2O_3, WC, TiC, and B_4C during the FSW/FSSW has been developed as an easy-to-implement to develop the strength and mechanical performance of joint samples due to their low coefficient of thermal expansion (CTE) [18–20]. Hong et al. [21] combined the friction stir spot welding with a nanoparticle deposition system of dissimilar aluminum alloys. They found that the mechanical performance of joints such as strength and toughness due to the formation of carbon/aluminum metal matrix composite improved clearly. Friction stir spot welding of Al and carbon fiber reinforced polymer was investigated by Ma et al [22]. It was shown that the maximum temperature at the Al alloy-CFRP interface improves as the plunge depth and rotational speed increase. Khorami et al. [23] analyzed the effect of SiC nanoparticles during the friction stir process of aluminum alloys. It was found that the young’s modulus, yield strength, and hardness in the stir zone improve due to the incorporation of SiC nanoparticles. The effect of SiC nanoparticles and mechanical vibration during the friction stir brazing of low carbon steel sheet with Sn-Pb filler material was investigated by Abbasi et al. [24]. They indicated that the distribution of SiC nanoparticles, mechanical performance, and microstructure refinement improve as mechanical vibration was applied during the joining process. The impact of nanoparticles on microstructure and mechanical performance of joints during friction stir spot welding was investigated by Sadeghi et al. [25]. It was clarified that the mechanical performances such as strength and hardness as well as microstructure refinement were totally improved as nanoparticle was added due to their coherent distribution in the matrix. Abdollahzadeh et al [26] applied the SiC nanoparticles during the friction stir process of magnesium alloys. The results indicated a

remarkable increase in mechanical characteristics, wear, and corrosion behaviors of processed samples as SiC particles were incorporated.

Up to now, little information is available on the impact of SiC nanoparticles on microstructural and mechanical evolution during friction stir spot welding of dissimilar alloys. The current examination was objected to analyzing the effect of SiC nanoparticles on microstructure and mechanical characteristics of FSSW-ed Al-Cu dissimilar alloys. The effect of joining parameters such as rotational speed and dwelling time was also analyzed. The production of spot joints with high quality and acceptable mechanical characteristics is the crucial aim of this research.

2. Experimental Procedure

Al 2024 and pure copper (C11000) sheets with 3 and 2 mm thickness, respectively were joined through FSSW. The nominal composition of the base materials is listed in Table 1. The workpieces were cut into 120 mm in length and 25 mm in width, and two sheets were joined on an overlap area of 25 × 25 mm^2 (Fig. 1(a)).

Table 1
Chemical composition of the analyzed Al and Cu determined via X-ray fluorescence (wt%)

Material/Element (wt%)	Ti	Si	Fe	Mn	Mg	Ag	Cr	Zn	Pb	As	Sb	Cu	Al
Al 2024	0.025	0.22	0.21	0.41	1.65	-	0.12	0.02	-	-	-	3.54	Bal
Copper	-	-	0.0009	-	-	0.0022	-	-	0.0005	0.0004	0.003	Bal	-

A welding tool fabricated of H13 steel, including a shank, shoulder, and pin, was applied during the joining (Fig. 1(b)). To omit any impurities and contamination, acetone was used. Firstly, two plates were placed on a steel backplate and then overlapped by 25 mm. The Al and Cu sheets were inserted tightly into the joining instrument by applying a fixture. SiC powder particles including a medium size of 50 nm with 99.9% purity were utilized as reinforcing particles in this study. In order to add the particles into the Al alloy matrix, a cube-shaped groove with a width and depth of 2×2 mm on the bottom of the aluminum sheet was first cut, and then the groove was filled with the SiC nanoparticle. After that, to encapsulate the particles within the specimen, the aluminum sheet with SiC powder was firstly processed by a pin-less tool, and then the aluminum specimen was welded to a copper sheet as shown in Fig. 1. To achieve the optimum welding parameters of rotational speed and dwell time, FSSW was done at rotational speeds of 1300, 1600, and 1900 rpm and dwell times of 2, 4, and 6 s. After the joining process, the specimens are applied to visual inspection, cross-sectional macrographs, microstructure analysis for the assessment of materials mixing, and mechanical tests such as hardness measurements. Regarding the cross-sectional macrographs and jointed zone's microstructure, the specimens are selected from the center of the zone.

Metallography analyses according to ASTM-E3-11 were used to detect the microstructure with optical microscopy (OM) equipped with quantitative image analysis software and scanning electron microscopy (SEM). For the aluminum sheet, an etchant consisting of HCl (2 mL), HF (2 mL), water (50 mL), HNO_3 (0.3 mL) was applied for 12 s, while this solution is contained HNO_3 (50 ml), $AgNO_3$ (0.5 ml), and water (50 ml) which used for 4 s. The linear intercept technique was utilized for calculating grain size in the various stir zone. Energy dispersive spectroscopy (EDS) and X-ray diffraction (XRD) with high resolution to analyze the IMCs at the stir zones of Al–Cu dissimilar joints applying a step size of 2∘/min and the scanning range of 30–100∘ were used. A tensile shear test was done on the joining specimens at ambient temperature with a crosshead speed of 2 mm/min based on the JIS Z 3136: 1999 standard. To improve the accuracy of obtained results, three measurements were calculated as shear failure load for each sample. Hardness distribution was calculated using the Vickers microhardness test across the joining line based on ASTM-E84-11 applying a load of 100 gf and a loading time of 10 s. An image analyzer software “Image J” in order to study the thickness and the void volume fraction of the reaction layer fabricated at the weld interface of the specimens was utilized.

3. Result And Discussion

3.1 Macrostructure analysis

The keyhole and flash are common phenomena during the FSSW process observed in all specimens. Figure 2 shows the cross-section morphologies with different magnification images of the joint at different rotational speeds and dwell times. In the stir zone (SZ),

owing to the extrusion and stirring implemented by the pin tool, a Cu hook has been extruded upward from the lower copper sheet into the upper aluminum sheet (known as Cu-ring). This Cu-ring leads to interlocking between the two materials and results in adherence of dissimilar alloys during the joining process, and consequently, reaches a high strength before failure during tensile testing [27]. Based on the rotational speed and dwelling time, the shape of the hook changed during the joining process. Table. 2 presents the width of the weld zone of Al-Cu dissimilar welding under different rotational speeds and dwell times. At a dwell time of 2 s with a rotational speed of 1300 rpm, metals are not able to be fully softened and therefore only plastic flow happened in a small scope, leading to a small stir zone (SZ). The size of the weld zone expanded as rotational speed and dwell time improved (Fig. 2b and 2c). Wang et al. [28] showed that rotational speed is a prominent role to play in the thermal cycles of the joints and resulting in a wider weld zone. With the increase in rotational speed and dwell time, the amount of nanoparticle and copper elements in the stir zone increases resulting in the formation of laminated bands of wider size in the stir zones. Figure 2(d) briefly discusses the geometric parameters of the hook during the welding process under various conditions. As observed in this figure, hook height (HH) indicates the distance from the tip of the hook to the interface layer of the joint. A fully bonded region (FBR) is related to the horizontal distance between the margin of the exit hole and the tip of the hook. The ratio of hook height to FBR is signified as HH/FBR, and the larger HH/FBR the steeper copper hook penetrated into the aluminum plate resulting in a stronger interlocking between the dissimilar alloys. Table. 3 presents the quantitative analyses of the geometric parameters of the hook at various rotational speeds and dwell times. It is observed from the data that the geometric parameters increase as rotational speed and dwell time increase because of the high heat input, thermomechanical flow, and heterogeneous mixing. In addition, the effect of rotational speed compared to the dwelling time is obvious due to higher heat input from the rotating tool during the joining process. However, the HH/FBR dropped dramatically as the rotational speed and dwell time further increased to 1900 rpm and 6 s, respectively because of the curling of the hook [29].

Table 2
The width of the joining zone for different rotational speeds and dwell time.

Dwell time : 2 (s)				**Dwell time : 4 (s)**			**Dwell time : 6 (s)**		
Rotational speed (rpm)	**1300**	**1600**	**1900**	**1300**	**1600**	**1900**	**1300**	**1600**	**1900**
Width (µm)	552	667	686	862	873	1112	1400	1810	2021

Table 3
Geometric parameters of the joints at various rotational speeds and dwell time.

Joining parameters		**HH (µm)**	**FBR (µm)**	**HH/FBR**
Rotational speed	**1300**	356.12	1211.63	0.2939
(rpm)	**1600**	572.84	1426.83	0.4014
	1900	317.81	1026.47	0.3096
Dwelling time	**2**	356.12	1211.63	0.2939
(s)	**4**	519.23	1364.95	0.3804
	6	304.26	983.84	0.3092

The top surface morphology of the weld joints with various rotation speeds and welding times is shown in Fig. 3. The quality of the weld zone in all samples is acceptable due to thermal conductivity inside the joint region improved, hence the forming property of the joint improves due to an increase in heat conduction. Furthermore, all top surfaces of joints have a shallow spot weld indentation in the stir zone (SZ) indicating the lowest position of the topography and a distinct flash of certain height at the outer edges of the joints. Due to the impression of the shoulder on the surface during the FSSW process, the formation of the flash is common. It has been accepted that elevated temperatures and high plastic deformation occurred as the heat input is increased during the joining process, resulting in the outward extension of the weld zone [30–32]. As shown in Fig. 3, the volume of the flash improved with rotational speed and joining time because of high friction heat and plastic strain. In terms of material flow, the materials at the top surface of the sheet (aluminum) flow in the tool rotation direction, and then this flow behavior has been transmitted downwards, consequently, a similar flow behavior happened in the bottom material (copper). During the welding with low heat input (rotational speed of 1300 and dwelling time of 2), the material flow is not sufficient to mix and joint dissimilar alloys owing to the high thermal conductivity of copper [33], consequently, the copper does not produce enough heat to soften the aluminum to generate sound joint. The intensity and

area of the material flow enhanced as the underlying materials moved which have been driven by the materials above with the improvement of rotational speed and dwelling time.

3.2 Microstructure

It has been known that the input heat plays a vital role in the grain softening or grain hardening during the welding process. The grains undergo grain hardening or freezing and softening if the amount of heat generated is less and high, respectively [34–36]. Worth mentioning is that the quality weld of aluminum and copper dissimilar joints is determined not only by the macrostructure behavior but also by the interior quality of the joint. The optical microstructures of the stir zone (SZ) in the Al-Cu dissimilar joints are shown for the aluminum side and copper side of the weld in Figs. 4 and 5 under different welding conditions. Tables 4 and 5 summarized the grain size of the weld zone for three certain regions including the heat-affected zone (HAZ), thermos-mechanically affected zone (TMAZ), and stir zone (SZ) for both aluminum and copper sides of Al-Cu dissimilar welding under different joint conditions. It is obvious from figures. 4 and 5 that the grains in the stir zone increase as rotational speed and dwell time increase. It should be mentioned that FSW/FSSW is assumed to be a hot deformation process because of the presence of heat and deformation simultaneously during the welding. Therefore, the restoration mechanism of dynamic recrystallization is common during FSW/FSSW of various metals and alloys [37–39]. During this condition, low angle grain boundaries (LAGBs), because of severe plastic deformation and high heat generated by welding rotational tool changed to high angle grain boundaries (HAGBs) during the FSSW process. Therefore, the nucleation of new grain in preferred places in the matrix is possible resulting in grain size reduction [40–43]. Worth mentioning is that reinforcing particles play a significant role in microstructure refinement. That is, SiC nanoparticles restrict the movement of grain boundaries by pinning effect mechanism resulting in a reduction in grain growth. Based on the movement rate of grain boundary (V) equation [44]:

$$V = M\exp\left(-\frac{Q}{R_g T}\right)\left(P_{dis} - P_z \pm P_c\right)$$

$$P_z = \frac{3f_v \gamma_{AB}}{4r}$$

1

where M is a constant, Q is related to the apparent activation energy, T is the temperature, P_{dis} indicates the required force with respect to recrystallization and is evaluated as a function of Burgers vector (b), shear modulus (G), and dislocation density (q) as 0.5 qGb2, P_z is related to the Zener pinning pressure, P_c is associated with the geometrical required force owing to the curvature of the grain boundaries, f_v and r are respectively related to volume fracture and radius of the particle, and γ_{AB} indicates the grain boundary tension. Karthikeyan and Mahadevan [45] studied the role of SiC nanoparticle addition in the joint zone during the FSW process. They showed that the nanoparticle restricts the growth of grain boundary by pinning and leads to an improvement in the mechanical characteristics to an extent of 33% in the as-welded condition over plain alloy. In addition, it has been known that reinforcing particles break up the initial grains into fine grains [46–48]. A similar mechanism with respect to the addition of SiC nanoparticles is observed in dissimilar Al-Mg joint alloys during the friction stir welding process [49]. SiC nanoparticles prevent the movement of the dislocation and grain boundary by pinning effect and also improved the recrystallization process owing to the development of nucleation sites. Regarding heat generation, owing to the friction between the rotating tool and workpiece as the main source of heat, the highest amount of heat is generated resulting in the annealing of metals. Consequently, the grain size increases in the stir zone. In other words, the heat input is at a high level while the cooling rate is at a low level as rotational speed and dwell time are increased, so there is sufficient energy and time with respect to recrystallized grains to grow.

From the distribution of nanoparticles, the tendency of SiC particles to agglomeration, owing to the high surface region, is high resulting in a reduction of their overall energy. The occurrence of agglomeration leads to an increase in inter-particle spacing to generate pores [50]. As observed in Fig. 4, the distribution of SiC in the matrix improves as rotational speed and dwell time decrease due to adequate input heat and time for break-up and interaction of reinforcing particles and matrix. These large reinforcing agglomerates are not able to pin the grain boundaries, consequently, they have no effective influence on the grain refinement of microstructure. Similar results were reported in the welding of dissimilar alloys with SiC nanoparticles by Moradi et al. [51]. They

indicated the fact that there is a homogenous mixing action between SiC reinforcing particles with aluminum matrix without a cluster of nanoparticles due to the used optimized welding parameters.

Table 4
The grain size of three main zones of weld joint on Al side after welding.

Dwell time : 2 (s)					Dwell time : 4 (s)			Dwell time : 6 (s)		
Rotational speed (rpm)		1300	1600	1900	1300	1600	1900	1300	1600	1900
Grain size (μm)	SZ	14.5	14.6	15.2	14.6	14.9	15.8	14.9	16.1	16.8
	TMAZ	38.8	39.7	40.04	39.1	40.12	43.3	40.5	42.1	45.4
	HAZ	62.05	63.05	63.8	62.7	63.05	64.12	63.8	64.0	65.21

Table 5
The grain size of three main zones of weld joint on Cu side after welding.

Dwell time : 2 (s)					Dwell time : 4 (s)			Dwell time : 6 (s)		
Rotational speed (rpm)		1300	1600	1900	1300	1600	1900	1300	1600	1900
Grain size (μm)	SZ	10.5	11.6	12.2	11.02	11.8	12.7	11.9	13.2	14.4
	TMAZ	35.8	36.7	37.04	36.2	37.1	39.3	37.5	38.2	41.2
	HAZ	39.05	40.5	43.09	41.7	42.5	44.1	42.4	43.0	45.1

3.3 Intermetallic compounds (IMCs) formation

The formation of brittle and hard intermetallic compounds (IMCs) layers in the FSSW process of dissimilar aluminum alloy and pure copper has been considered one of the most critical factors affecting the mechanical performance of joints [52]. In this condition, detachment of copper pieces from the copper alloy and distribution with aluminum matrix results in the formation of IMCs by the solid-state diffusion in the stir zone. Worth noticing is that temperature, strain rate, welding parameters, chemical compositions, and time have been considered the fundamental parameters in the formation of such [53–55]. Zuo et al. [56] investigated the role of IMCs formation in mechanical behaviors of weld joints during the dissimilar Al-Cu joint. It was found that three certain reaction layers namely AlCu, $AlCu_2$, and Al_2Cu/α-Al eutectic layer are formed at the Cu/Al welding interface. In addition, the thickness of the Al_2Cu/α-Al eutectic layer increases, unlike the thickness of the continuous Al_2Cu layer, as ultrasonic vibration is applied during the joining process. Xue et al. [57] optimized the joining parameters and indicated that in order to achieve a sound joint, a thin and continuous IMC layer at the interface joint is required. SEM images for the Al-Cu interface at the various rotational time and dwell times are shown in Figs. 6–8. It has been observed that the thickness of IMCs during the FSSW process increases as rotational speed and dwell time increase due to high interaction between Al and Cu materials. It should be noticed that a proper thickness joint is related to sufficient fluidity and stir in the weld zone resulting in good wettability of the weld layer on the Al-Cu substrates. Therefore, this phenomenon enhances the diffusion of Al and Cu atoms at the solid interfaces to fabricate strong Al-Cu metallurgical joints. The micro-crack at the interface joint of Al-Cu dissimilar welding is observed at high dwell time and rotational speed. This phenomenon may be associated with the dissimilarity in thermal expansion coefficients between IMCs and matrix resulting in incongruous deformation during the cooling process [58–60]. Liu et al. [61] indicated that the continued intermetallic compounds layers can lead to fast crack propagation during mechanical studies such as tensile shear tests. The EDS analysis results for possible IMCs in different zones are presented in Table. 6. Moreover, the XRD outcomes from the cross-section of the relevant weld samples are shown in Fig. 9 which verifies the EDS data. It is clear that the expanding of the IMC layer at the weld interface under high rotational speed and dwell time may be associated with the combined influences of higher heat input and severe plastic deformation. In all, the increase in the IMC formation at the joint interface shows variant trends of behaviors. Higher aluminum contents detected in the EDX spot examination of the weld interfaces could be owing to various factors such as the lower melting point of aluminum alloys compared to the copper alloys and welding tool pin offset towards the softer materials (aluminum) [62]. From Table. 6, the content of Si particles increases in the interface zone as the rational speed and dwell time increase during the FSSW process. This phenomenon may be attributed to the temperature effect on particle agglomeration. Bagheri et al. [63] indicated the fact that the SiC particles show a high tendency to formation of agglomeration at high-temperature values. It is proper to say that constant variation in different variables including time, complex grain nature, and temperature severely influences the formation of intermetallic compounds and expansion, and hence, transform the possible IMC [64].

Furthermore, the EDX spot analysis and EDX line scan are two distinct techniques applied in recognizing local chemical contents and elemental distribution of the aluminum and copper at the interfaces, respectively. However, the fundamental discrepancies in the joint interface depend on the thickness of the expanded IMC layer at each dwell time and rotational speed. Al-rich IMC layers improved in all welding conditions are AlCu and Al_2Cu, while in the interface region, Al_2Cu is the dominant IMC layer. Worth mentioning is that the formation of Al_2Cu happens wherever adequate atomic concentrations have been locally achieved which is an important issue in terms of the therrmomechanically induced solid-state diffusion process. It has been also known as the most important IMCs layer in the Al-Cu system [65]. Based on results in Fig. 9, no Cu_9Al_4 was detected in the aluminum-copper interface under various welding conditions, unlike the previous studies. Bhattacharya et al. [66] reported the formation of this phase in the interface joint during FSW of HCP Cu and AA6063 dissimilar alloys. They found that the formation of the Cu_9Al_4 phase happened at high-peak temperature with high formation energy compared with $CuAl_2$ and CuAl phases. Ouyang et al. [67] reported the occurrence of this phenomenon at the bottom of the stir zone due to mechanical integration. However, the absence of Cu_9Al_4 formation in this study can be associated with two critical reasons: Firstly, the heat input in Al-Cu alloys is exactly enough to plasticize the materials; and secondly, the peak temperature value under all welding conditions is lower than the formation temperature of this phase. These outcomes are in accordance with results reported by Fei et al. [68].

Table 6
The EDS analysis results for possible IMCs in different zones detected in Figs. 6–8.

Rotational speed : 1300 (rpm)					Rotational speed : 1600 (rpm)			Rotational speed : 1900 (rpm)		
Dwell time (s)/Point		2	4	6	2	4	6	2	4	6
P_1	Al (%wt)	87.12	84.18	82.73	84.09	83.26	80.03	81.63	79.78	77.12
	Cu (%wt)	4.61	5.03	5.24	5.02	5.53	6.73	6.04	6.63	7.04
	Si (%wt)	8.27	10.78	12.03	10.89	11.21	13.24	12.33	13.59	15.84
P_1	Al (%wt)	39.12	38.38	37.63	41.88	39.52	38.12	40.89	40.03	39.03
	Cu (%wt)	35.63	34.89	34.12	37.52	36.29	35.34	38.02	37.58	36.47
	Si (%wt)	25.25	26.73	28.25	20.06	24.19	26.54	21.09	22.39	24.50
P_3	Al (%wt)	8.16	8.89	9.11	8.67	9.28	12.88	11.26	11.87	11.96
	Cu (%wt)	81.26	79.47	77.31	79.18	76.25	73.49	78.52	76.11	76.49
	Si (%wt)	10.58	11.64	13.58	12.15	14.47	13.63	10.22	12.02	11.55

Fundamentally, Eq. (2) has been used to measure the thickness of the IMCs layer during thermal processing [69]:

$$W = kt^n \quad (2)$$

where W relates to the intermetallic thickness, k is the growth rate constant, n indicates the time exponent, and t expresses the thermal processing time. Several studies have reported that the IMCs show two distinct forms of solid-phase growth [70]. The first has been known the linear growth and the other has been known the parabolic growth. The linear growth rate is associated with the reaction rate of the growth interface. Parabolic growth is dependent on bulk diffusion. For IMCs layers with the parabolic growth mechanism, the value of n is 0.5 [71]. Figure 10 shows the variation of the interfacial IMCs layers thickness and void volume percentage regarding rotational speeds and dwell time for joint interfaces. It is clear from the results that the thickness of IMCs and void volume percentage in joints increase with an improvement in the rotational speed and dwell time. With the increase in rotational speed, the friction between the shoulder and the welding sample increases, therefore due to higher heat, the fluidity of the material in the interface increases resulting in acceleration of the atom diffusion to form IMCs layers. Given the long interaction between the FSSW tool and the workpiece at a high dwelling time, the frictional heat enhances causing the formation of large IMCs and stick of them to the welding tool or the workpiece. In other words, a higher welding temperature because of high rotational speed leads to the formation of a high-thick reaction layer.

3.4 Mechanical properties

Table. 7 presents the shear test results of joint samples under different welding conditions. According to these results, the shear strength of weld specimens increases as rotational speed and dwell time increase. This phenomenon may be associated with the formation of IMCs layers, as well as reinforcing particles' role as mentioned in the microstructural evolution section. Worth mentioning that reinforcing particles in the formation of the IMCs layer are vital to the strength of weld samples. That is, the interaction between reinforcing particles and base metals, degree of particle distribution, and agglomeration in the matrix, as well as the interfacial bond between reinforcing particles and base metals, influences the strength properties [72, 73]. Adding the SiC nano-particle reinforcing leads to the transfer of the applied tension from the weak matrix into the strong reinforcing particle, resulting in an improvement of the strength. In other words, due to an incoherent reinforcement-matrix interface, load-bearing capacity could be improved between the base matrix and reinforcing agent in the composite structure. With increasing the input heat by increasing rotational speed or dwell time, the required energy for the formation of brittle intermetallic compounds is supplied. The IMC layer, at the lowest rotational speed and dwell time, formed discontinuously with low thickness at the joint interface, resulting in the weak metallurgical combination of the intermetallic. This phenomenon leads to a decrease in the tensile shear failure load of the joint. The continuous IMC layer with high thickness is formed as rotational speed and dwell time increase due to high input heat. Therefore, the weld zone is mechanically and metallurgically bonded which is studied in previous studies [74, 75]. In addition, SiC nanoparticle has been considered a prominent factor in impact energy absorption and dislocation destiny in weld samples due to mismatch in thermal coefficient [76].

The relationship between tensile shear failure load and the heat generation for weld specimens under different rotational speeds and dwell time is presented in Fig. 12. As shown, the load tensile shear increase as the heat generation is increased. This can be associated with the heat generation affected by the formation of the IMCs layer. These results indicate the fact that the range of used values for welding parameters is optimal with high mechanical properties. That is, the formation and thickness of IMCs at the joint interface do not show a negative effect on the quality of weld samples and play a positive role in the mechanical properties of joint specimens during the FSSW of Al-Cu alloys.

Table. 7 presents the microhardness profile of weld samples under different rotational speeds and dwell times. As seen, the microhardness values of joints increase as rotational speed and dwell time increase. It has been known that hardness mainly depends on the intermetallic formation, grain size, and density of dislocations in the weld region [76]. To be more specific, based on the Hall – Petch equation, there is a relationship between grain size and the microhardness profile of the joining zone to generate the dislocations because of the discrepancies between thermal expansion coefficients of base metal and reinforcing nano-particles. The introduction of reinforcing nano-particles due to the hard nature of SiC particles as well as the pinning effect of the grain boundaries results in an increase in microhardness. From the IMCs aspect, the high input heat due to an increase in rotational speed and dwell time, the formation of the IMCs is enhanced, so the microhardness is increased [77]. The stir zone, due to a high level of materials mixing between different elements and the formation of IMCs because of high-temperature values, shows higher hardness behaviors compared to two other regions (TMAZ and HAZ). Furthermore, large bulky copper fragments in the center zone of the weld region are reported by Mehta et al. [10] in which the level of severe plastic deformation, as well as strain hardening during the thermomechanical process, is high. It can be concluded from mechanical behaviors of weld samples with various rotational speeds and dwell time that the formation and thickness of continuous IMCs layer have a more prominent impact on the strength and hardness of the weld zone.

Table 7
Hardness profile of joint samples under different rotational speeds and dwell time. A) 1300 rpm, b) 1600 rpm, and c) 1900 rpm.

Rotational speed : 1300 (rpm)					**Rotational speed : 1600 (rpm)**			**Rotational speed : 1900 (rpm)**		
Dwell time (s)		**2**	**4**	**6**	**2**	**4**	**6**	**2**	**4**	**6**
Hardness	**SZ**	122 ± 2	126 ± 2	132 ± 2	127 ± 2	133 ± 2	142 ± 2	131 ± 2	149 ± 2	156 ± 2
(HV)	**TMAZ**	95 ± 2	98 ± 2	105 ± 2	115 ± 2	121 ± 2	134 ± 2	123 ± 2	131 ± 2	143 ± 2
	HAZ	74 ± 2	77 ± 2	82 ± 2	91 ± 2	98 ± 2	123 ± 2	104 ± 2	119 ± 2	125 ± 2

4. Conclusion

According to the obtained results, it was shown that friction stir spot (FSSW) of Al 2024-Cu dissimilar joints under different rotational speeds and dwell time with SiC nanoparticles could be done successfully. In the current article, the micro-macrostructure of the weld

zone, formation of intermetallic compounds, tensile strength, and micro-hardness of the joints were analyzed. According to the obtained results, the following conclusions could be reported:

1- Increasing input heat due to high rotational speed and dwell time, resulting in grain size improvement. The grain sizes of Al and Cu in the stir zone were increased from 14.5 and 10.5 to 62.2 and 45.1 μm, respectively.

2- The geometric parameters of weld samples increase as rotational speed and dwell time increase because of the high heat input, thermomechanical flow, and heterogeneous mixing.

3- The thickness of IMCs during the FSSW process increases as rotational speed and dwell time increase due to high interaction between Al and Cu materials. The formation of AlCu and Al_2Cu intermetallic compounds in SZ was analyzed.

4- The highest tensile shear failure load was obtained in joints prepared by 1900 rpm rotation speed and 6 s dwell time, as it was 3300 N. This can be associated with the heat generation affected the formation of the IMCs layer.

5- The microhardness values of the joint increase from 122 to 156 Hv as rotational speed and dwell time increase due to the intermetallic formation and density of dislocations in the weld region.

Declarations

Acknowledgement

Authors reveal their cordial gratefulness and admiration to Amirkabir University of Technology for providing components and a working place.

Contributions

Idea and design of the study: Ali Shamsipur, Seyyed Ehsan Mirsalehi; Conducting of experiments: Mehdi Alizadeh, Behrouz Bagheri; Data acquisition: Mehdi Alizadeh, Behrouz Bagheri, Amin Abdollahzadeh; Writing, Analysis of data: Behrouz Bagheri, Amin Abdollahzadeh; Final review and editing the manuscript: Behrouz Bagheri, Seyyed Ehsan Mirsalehi.

Ethics declarations

This research follows ethical standards.

Funding

This research did not receive any specific grant from funding agencies in the public, commercial, or not-for-profit sectors.

Declaration of Competing Interest

I would like to declare on behalf of all the authors that the authors declare no competing interests.

Consent to Participate and publish

The article is an original research completed by all the authors. All authors have willingly participated in this paper. All the co-authors agree to publish this article. Furthermore, this article has not been published in any other journals.

Data availability

All data generated or analyzed during this investigation are available in this research article.

References

1. Mehta KP, Badheka VJ (2017) Influence of tool pin design on properties of dissimilar copper to aluminum friction stir welding. Trans Nonferrous Met Soc China 27:36–54. https://doi.org/10.1016/S1003-6326(17)60005-0

2. Jafari M, Abbasi M, Poursina D, Gheysarian A, Bagheri B (2017) Characterization of microstructure and mechanical properties of dissimilar steel- copper joint made by FSW. J Mech Sci Technol 31(3):1135–1142
3. Memon S, Paidar M, Mehta KP, Babaei B, Lankarani HM (2021) Friction spot extrusion welding on dissimilar materials AA2024-T3 to AA5754-O: effect of shoulder plunge depth. J Mater Eng Perform 30:334–345. https://doi.org/10.1007/s11665-020-05387-4
4. Carlone P, Astarita A, Palazzo GS, Paradiso V, Squillace A (2015) Microstructural aspects in AleCu dissimilar joining by FSW. Int J Adv Manuf Technol 79:1109–1116. https://doi.org/10.1007/s00170-015-6874-z
5. Mahmoud Abbasi M, Givi B, Bagheri (2020) New Method to Enhance the Mechanical Characteristics of Al-5052 Alloy Weldment Produced by Tungsten Inert Gas, Proceedings of the Institution of Mechanical Engineers: Part B Journal of Engineering Manufacture, https://doi.org/10.1177/0954405420929777
6. Li XW, Zhang DT, Qui C, Zhang W (2012) Microstructure and mechanical properties of dissimilar pure copper/1350 aluminum alloy butt joints by friction stir welding. Trans Nonferrous Metals Soc China 22:1298–1306. https://doi.org/10.1016/S1003-6326(11)61318-6
7. Weigl M, Albert F, Schmidt M (2011) Enhancing the ductility of laser-welded copper-aluminum connections by using adapted filler materials. Phys Procedia 12:332–338. https://doi.org/10.1016/j.phpro.2011.03.141
8. Patel NP, Parlikar P, Dhari RS, Mehta K, Pandya M (2019) Numerical modelling on cooling assisted friction stir welding of dissimilar Al-Cu joint. J Manuf Process 47:98–109. https://doi.org/10.1016/j.jmapro.2019.09.020
9. Mehta KP, Badheka VJ (2016) A review on dissimilar friction stir welding of copper to aluminum: process, properties, and variants. Mater Manuf Process 31:233–254. https://doi.org/10.1080/10426914.2015.1025971
10. Kush Mehta A, Astarita P, Carlone RD, Gatta H, Vyas P, Vilaca F, Tucci (2021) Investigation of exit-hole repairing on dissimilar aluminum-copper friction stir welded joints. J Mater Res Technol 13:2180–2193. https://doi.org/10.1016/j.jmrt.2021.06.019
11. Rasoul, Keivani Behrouz. Bagheri, Farzaneh. Sharifı, Mostafa. Ketabchi, Mahmoud. Abbasi, Effects of pin angle and preheating on temperature distribution during friction stir welding operation,Transaction of Nonferrous Metals Society of China, Vol 23(9), 2013, pp 2708 – 2713. https://doi.org/10.1016/S1003-6326(13)62788-0
12. Behrouz Bagheri M, Abbasi M, Dadaei (2020) Mechanical behavior and microstructure of AA6061-T6 joints made by friction stir vibration welding. J Mater Eng Perform 29:1165–1175. https://doi.org/10.1007/s11665-020-04639-7
13. Behrouz Bagheri F, Sharifi M, Abbasi A, Abdollahzadeh (2022) On the Role of Input Welding Parameters on the Microstructure and Mechanical Properties of Al6061-T6 Alloy during the Friction Stir Welding: Experimental and Numerical Investigation, Proceedings of the Institution of Mechanical Engineers Part L Journal of Materials Design and Applications, Vol 236(2), pp. 299–318. https://doi.org/10.1177/14644207211044407
14. Fujun Cao J, Li W, Hou Y, Shen R, Ni (2021) Microstructural evolution and mechanical properties of the friction stir welded Al–Cu dissimilar joint enhanced by post-weld heat treatment. Mater Charact 174:110998. https://doi.org/10.1016/j.matchar.2021.110998
15. FELIX XAVIER MUTHU M (2016) Effect of pin profile and process parameters on microstructure and mechanical properties of friction stir welded Al – Cu joints. Trans Nonferrous Met Soc China 26 984 – 993. https://doi.org/10.1016/S1003-6326(16)64195-X
16. Esther TAKINLABI, Anthony ANDREWS, Stephen A, AKINLABI (2014) Effects of processing parameters on corrosion properties of dissimilar friction stir welds of aluminium and copper. Trans Nonferrous Met Soc China 24 1323 – 1330. https://doi.org/10.1016/S1003-6326(14)63195-2
17. Garg A (2017) Bhattacharya, Anirban, Similar and Dissimilar Joining of AA6061-T6 and Copper by Single and Multi-spot Friction Stirring. J Mater Process Technol. http://dx.doi.org/10.1016/j.jmatprotec.2017.07.029
18. Behrouz Bagheri A, Abdollahzadeh F, Sharifi M, Abbasi (2021) The Role of Vibration and Pass Number on Microstructure and Mechanical Properties of AZ91/SiC Composite Layer during Friction Stir Processing, Proceedings of the Institution of Mechanical Engineers: Part C Journal of Mechanical Engineering Science, 1–15. https://doi.org/10.1177/09544066211024281
19. Behrouz Bagheri M, Abbasi A, Abdollahzadeh SE, Mirsalehi (2020) The Effect of Second Phase Particle Size and Presence of Vibration on AZ91/SiC Surface Composite Layer Produced by FSP. Trans Nonferrous Met Soc China 30:905–916. https://doi.org/10.1016/S1003-6326(20)65264-5
20. Mahmoud, Abbasi (2015) Amin. Abdollahzadeh, Behrouz. Bagheri, Hamid. Omidvar,. The effect of SiC particle addition during FSW on microstructure and mechanical properties of AZ31 magnesium alloy International Journal Materials Engineering and

Performance 24(12):5037–5045. https://doi.org/10.1007/s11665-015-1786-5

21. Das Sung-TaeHHrishikesh, Oh H-S, Mohammad Nur E, Alam Al Nasim D-M, Chun (2017) Combination of nano-particle deposition system and friction stir spot welding for fabrication of carbon/aluminum metal matrix composite joints of dissimilar aluminum alloys. CIRP Annals - Manufacturing Technology. http://dx.doi.org/10.1016/j.cirp.2017.04.115
22. Ma N, Geng P, Ma Y, Shimakawa K, Choi J-W, Aoki Y, Fujii H (2021) Thermo-mechanical modeling and analysis of friction spot joining of Al alloy and carbon fiberreinforced polymer. Mater Res Technol. https://doi.org/10.1016/j.jmrt.2021.03.111
23. Sarkari Khorrami M, Saito N, Miyashitac Y, Kondo M (2019) Texture variations and mechanical properties of aluminum during severe plastic deformation and friction stir processing with SiC nanoparticles. Mater Sci Eng A 744:349–364. https://doi.org/10.1016/j.msea.2018.12.031
24. Mahmoud Abbasi B, Bagheri F, Sharifi A, Abdollahzadeh, Friction Stir Vibration Brazing (FSVB) (2021) An Improved Version of Friction Stir Brazing. Weld World 65(11):2207–2220. https://doi.org/10.1007/s40194-021-01173-5
25. Behzad Sadeghi H, Abbasi M, Atapour S, Shafiee P, Cavaliere, Marfavi Z (2020) Friction stir spot welding of TiO2 nanoparticlereinforced interstitial free steel. J Mater Sci. https://doi.org/10.1007/s10853-020-04838-6
26. Amin Abdollahzadeh B, Bagheri M, Abbasi F, Sharifi AO, Moghaddam (2021) Mechanical, Wear and Corrosion Behaviors of AZ91/SiC Composite Layer Fabricated by Friction Stir Vibration Processing,. 9:1–17. https://doi.org/10.1088/2051-672X/ac2176.3
27. Heideman R, Johnson C, Kou S (2010) Metallurgical analysis of Al/Cu friction stir spot welding. Sci Technol Weld Joining 15(7):597–604. https://doi.org/10.1179/136217110X12785889549985
28. Wang Q, Zhao Z, Zhao Y, Yan K, Zhang H (2015) The adjustment strategy of welding parameters for spray formed 7055 aluminum alloy underwater friction stir welding joint. Mater Des 88:1366–1376. https://doi.org/10.1016/j.matdes.2015.09.038
29. Li G, Zhou L, Zhou W, Song X, Huang Y (2019) Influence of dwell time on microstructure evolution and mechanical properties of dissimilar friction stir spot welded aluminum–copper metals. J Mater Res Technol. https://doi.org/10.1016/j.jmrt.2019.02.015
30. Behrouz Bagheri M, Abbasi M, Dadaei, Journal (2020) Vol (9), pp33–46. https://doi.org/10.1007/s13632-019-00606-4
31. Oladimeji OO, Taban E, Kaluc E (2016) Understanding the role of welding parameters and tool profile on the morphology and properties of expelled flash of spot welds. Mater Des 108:518–528. http://dx.doi.org/10.1016%2Fj.matdes.2016.07.013
32. Behrouz Bagheri AAkbarM, Rizi M, Abbasi M, Givi, Friction Stir Spot Vibration Welding (2019) : Improving the Microstructure and Mechanical Properties of Al5083 Joint, Metallography, Microstructure, and Analysis Journal, Vol 8 (5), pp 713–725. https://doi.org/10.1007/s13632-019-00563-y
33. Jian WANG, Xiao-wei WANG, Bo LI, Cheng CHEN, Xiao-feng LU (2021) Interface repairing for AA5083/T2 copper explosive composite plate by friction stir processing. Trans Nonferrous Met Soc China 31 2585 – 2596. https://doi.org/10.1016/S1003-6326(21)65677-7
34. Li B, Shen Y, Luo L, Hu W (2013) Fabrication of TiCp/Ti-6Al-4V surface composite via friction stir processing (FSP): process optimization, particle dispersion-refinement behavior and hardening mechanism. Mater Sci Eng A 574:75–85. https://doi.org/10.1016/j.msea.2013.03.019
35. Mishra RS, Mahoney MW (2007)Friction Stir Welding and Processing; ASM International,
36. Yang Y, Zhao Y, Kai X, Tao R (2017) Superplasticity behavior and deformation mechanism of the in-situ Al3Zr/6063Al composites processed by friction stir processing. J Alloys Compd 710:225–233. https://doi.org/10.1016/j.jallcom.2017.03.246
37. Saleh Alaeibehmand SE, Mirsalehi E, Ranjbarnodeh (2021) Pinless FSSW of DP600/Zn/AA6061 dissimilar joints. J Mater Res Technol 15:996–1006. https://doi.org/10.1016/j.jmrt.2021.08.071
38. Saremi ML, Mirsalehi SE, Shamsipur A (2017) Investigation on metallurgical structure and mechanical properties of dissimilar Al 2024/Cu FSW T-joints. Trans Indian Inst Met 70(7):1869–1877. https://doi.org/10.1007/s12666-016-0991-8
39. Mahmoud Abbasi B, Bagheri A, Abdollahzadeh AO, Moghaddam (2021) A Different Attempt to Improve the Formability of Aluminum Tailor Welded Blanks (TWB) Produced by the FSW. IntJ Mater Form 14(5):1189–1208. https://doi.org/10.1007/s12289-021-01632-w
40. Farhad BAKHTIARIARGESI, Ali SHAMSIPUR, Seyyed Ehsan MIRSALEHI (2021) Preparation of bimetallic nano-composite by dissimilar friction stir welding of copper to aluminum alloy. Trans Nonferrous Met Soc China 31 1363 – 1380. https://doi.org/10.1016/S1003-6326(21)65583-8

41. Mahmoud Abbasi B, Bagheri F, Sharifi, Simulation and Experimental Study of Dynamic Recrystallization Process during Friction Stir Vibration Welding of Magnesium Alloys (2021) Trans Nonferrous Met Soc China 31:2626–2650. https://doi.org/10.1016/S1003-6326(21)65681-9
42. Saremi ML, Mirsalehi SE, Shamsipur A (2016) Investigation on Metallurgical Structure and Mechanical Properties of Dissimilar Al 2024/Cu FSW T-joints. Trans Indian Inst Met. https://doi.org/10.1007/s12666-016-0991-8
43. Amin Abdollahzadeh B, Bagheri M, Abbasi F, Sharifi SE, Mirsalehi, Ahmad Ostovari Moghaddam, A Modified Version of Friction Stir Welding Process of Aluminum Alloys (2021) : Analyzing the Thermal Treatment and Wear Behavior, Proceedings of the Institution of Mechanical Engineers Part L Journal of Materials Design and Applications, Vol 235(10), pp 2291–2309. https://doi.org/10.1177/14644207211023987
44. Amin Abdollahzadeh B, Bagheri M, Abbasi AH, Kokabi (2021) Ahmad Ostovari Moghaddam, Comparison of the Weldability of AA6061-T6 Joint Under Different Friction Stir Welding Conditions. J Mater Eng Perform 30:1110–1127. https://doi.org/10.1007/s11665-020-05379-4
45. Karthikeyan P, Mahadevan K (2015) Investigating on the Effects of SiC Particles Addition in the Weld Zone During Friction Stir Welding of Al 6351 Alloy. Int J Adv Manuf Technol. https://doi.org/10.1007/s00170-015-7160-9
46. ARGESI F B, SHAMSIPUR A, MIRSALEHI SE (2018) Dissimilar joining of pure copper to aluminum alloy via friction stir welding [J]. Acta Metall Sinica (EnglishLetters) 31:1183–1196. https://doi.org/10.1007/s40195-018-0741-5
47. Mahmoud Abbasi A, Abdollahzadeh B, Bagheri AO, Moghaddam F, Sharifi, Dadaei M (2021) Study the Effect of the Welding Environment on the Dynamic Recrystallization Phenomenon and Residual Stresses during the FSW Process of Aluminum Alloy, Proceedings of the Institution of Mechanical Engineers Part L Journal of Materials Design and Applications, Vol 235(8), pp 1809–1826. https://doi.org/10.1177/14644207211025113
48. Behrouz Bagheri M, Abbasi A, Abdollahzadeh AH (2020) Kokabi,. 90:2275–2296. https://doi.org/10.1007/s00419-020-01720-4. Numerical Analysis of Cooling and Joining Speed Effects on Friction Stir Welding by Smoothed Particle Hydrodynamics (SPH), Archive of Applied Mechanics Journal, Vol (
49. Tabasi M, Farahani M, Givi MKB, Farzami M, Moharami A (2016) Dissimilar friction stir welding of 7075 aluminum alloy to AZ31 magnesium alloy using SiC nanoparticles. Int J Adv Manuf Technol 86:705e15. https://doi.org/10.1007/s00170-015-8211-y
50. Maitra S, Roy J (2018) Nanoceramic matrix composites: types, processing, and applications. Elsevier Ltd. https://doi.org/10.1016/B978-0-08-102166-8.00003-7
51. Moradi MM, Jamshidi Aval H, Jamaati R, Amirkhanlou S, Ji S (2019) Effect of SiC nanoparticles on the microstructure and texture of friction stir welded AA2024/AA6061. Mater Char 152:169e79. https://doi.org/10.1016/j.matchar.2019.04.020
52. Najib A, Muhammad CS, Wu W, Tian (2019) Effect of ultrasonic vibration on the intermetallic compound layer formation in Al/Cu friction stir weld joints. J Alloys Compd 785:512e522. https://doi.org/10.1016/j.jallcom.2019.01.170
53. Zhang J, Shen Y, Yao X, Xu H, Li B (2014) Investigation on dissimilar underwater friction stir lap welding of 6061-T6 aluminum alloy to pure copper. Mater Des 64:74e80. https://doi.org/10.1016/j.matdes.2014.07.036
54. Galvao I, Oliveira JC, Loureiro A, Rodrigues DM (2012) Formation and distribution of brittle structures in friction stir welding of aluminium and copper: influence of shoulder geometry. Intermetallics 22:122–128. https://doi.org/10.1016/j.intermet.2011.10.014
55. Mehta KP, Badheka VJ (2017) Hybrid approaches of assisted heating and cooling for friction stir welding of copper to aluminum joints. J Mater Process Technol 239:336e345. https://doi.org/10.1016/j.jmatprotec.2016.08.037
56. Zuo YY, Gong P, Ji SD, Li QH, Ma ZW, Lv Z (2021) Ultrasound-assisted friction stir transient liquid phase spot welded dissimilar copper-aluminum joint. J Manuf Process 62:58–66. https://doi.org/10.1016/j.jmapro.2020.11.019
57. Xue P, Xiao BL, Ma ZY (2015) Effect of interfacial microstructure evolution on mechanical properties and fracture behavior of friction stir-welded Al–Cu joints. Metall Mater Trans A 46(7):3091–3103. https://doi.org/10.1007/s11661-015-2909-1
58. Behrouz Bagheri M, Abbasi F, Sharifi (2021) Amin Abdollahzadeh, Investigation into Novel Multipass Friction Stir Vibration Brazing of Carbon Steels,. https://doi.org/10.1080/10426914.2021.2006220.
59. Tan CW, Jiang ZG, Li LQ, Chen YB, Chen XY (2013) Microstructural evolution and mechanical properties of dissimilar Al–Cu joints produced by friction stir welding. Mater Des 51(5):466–473. http://dx.doi.org/10.1016%2Fj.matdes.2013.04.056
60. Vahid S, Rizi M, Abbasi (2021) Behrouz. Bagheri, Investigation on Intermetallic Compounds Formation and Effect of Reinforcing Particles during Friction Stir Vibration Brazing. J Mater Eng Perform 1–13. https://doi.org/10.1007/s11665-021-06443-3

61. Jinglin Liu Q, Song L, Song S, Ji M, Li Z, Jia K, Yang (2020) A Novel Friction Stir Spot Riveting of Al/Cu Dissimilar Materials. Acta Metall Sinica (English Letters). https://doi.org/10.1007/s40195-020-01092-2
62. Kundig KJA, Weed RD (2015) Copper and copper alloys. In: Kutz M (ed) Mech. Eng. Handb. fourth ed., John Wiley & Sons Inc, Hoboken, New Jersey, pp 117–227. https://doi.org/10.1002/9780470172551.ch5
63. Behrouz Bagheri M, Abbasi A, Abdollahzadeh AH, Kokabi (2020) A comparative study between friction stir processing and friction stir vibration processing to develop magnesium surface nanocomposite. Int J Min Metall Mater 27:1133–1146. https://doi.org/10.1007/s12613-020-1993-4
64. Rajan K, Wallach ER (1980) A transmission electron microscopy study of intermetallic formation in aluminium-copper thin-film couples. J Cryst Growth. https://doi.org/10.1016/0022-0248(80)90164-5
65. Curry BE (1907) The constitution of the aluminum bronzes. J Phys Chem 11:425e436. https://doi.org/10.1021/j150087a001
66. Ouyang J, Yarrapareddy E, Kovacevic R (2006) Microstructural evolution in the friction stir welded 6061 aluminum alloy (T6-temper condition) to copper. J Mater Process Technol 172:110–122. https://doi.org/10.1016/j.jmatprotec.2005.09.013
67. Bhattacharya TK, Das H, Pal T (2015) Influence of welding parameters on material flow, mechanical property and intermetallic characterization of friction stir welded 6063 AA to HCP copper dissimilar butt joint without offset. Trans Nonferrous Met Soc China 25(9):2833–2846. http://dx.doi.org/10.1016/S1003-6326(15)63909-7
68. Fei X, Ye Y, Jin L, Wang H, Lv S (2010) Special welding parameters study on Cu/Al joint in laser-heated friction stir welding. J Mater Process Technol. https://doi.org/10.1016/j.jmatprotec.2018.02.004
69. Shen J, Zhao ML, He PP, Pu YY (2013) Growth behaviors of intermetallic compounds at Sn–3Ag–0.5Cu/Cu interface during isothermal and non-isothermal aging. J Alloys Compd 574:451–458. https://doi.org/10.1016/j.jallcom.2013.05.156
70. Hu XW, Li YL, Min ZX (2014) Interfacial reaction and IMC growth between Bi-containing Sn0.7Cu solders and Cu substrate during soldering and aging. J Alloys Compd 582:341–347. https://doi.org/10.1016/j.jallcom.2013.08.018
71. Kim DG, Jung SB (2005) Interfacial reaction and growth kinetics for intermetallic compounds layer between In-Sn solder and bare Cu substrate. J Alloys Compd 386:151–156. https://doi.org/10.1016/j.jallcom.2004.05.055
72. Behrouz Bagheri M, Abbasi A, Abdollahzadeh (2021) Microstructure and Mechanical Characteristics of AA6061-T6 Joints Produced by Friction Stir Welding, Friction Stir Vibration Welding and Tungsten Inert Gas Welding: A Comparative Study. Int J Min Metall Mater 28(3):450–461. https://doi.org/10.1007/s12613-020-2085-1
73. BODAGHI M, DEHGHANI K (2017) Friction stir welding of AA5052: The effects of SiC nano-particles addition [J]. Int J Adv Manuf Technol 88:2651–2660. https://doi.org/10.1007/S00170-016-8959-8
74. Yazdipour A, Heidarzadeh A (2016) Effect of friction stir welding on microstructure and mechanical properties of dissimilar Al 5083-H321 and 316L stainless steel alloy joints. J Alloy Compd 680:595–603. https://doi.org/10.1016/j.jallcom.2016.03.307
75. Zhou L, Li GH, Zhang RX, Zhou WL, He WX, Huang YX, Song XG (2018) Microstructure evolution and mechanical properties of friction stir spot welded dissimilar aluminum copper joint. J Alloys Compd. doi: https://doi.org/10.1016/j.jallcom.2018.10.045
76. Xia-wei LI, Da-tong ZHANG, Cheng QIU, Wen ZHANG (2012) Trans Nonferrous Met Soc China 22:1298–1306. https://doi.org/10.1016/S1003-6326%2811%2961318-6. Microstructure and mechanical properties of dissimilar pure copper/1350 aluminum alloy butt joints by friction stir welding [J]
77. KARAKIZIS P, PANTELIS D, FOURLARIS G (2018) Effect of SiC and TiC nanoparticle reinforcement on the microstructure, microhardness, and tensile performance of AA6082-T6 friction stir welds [J]. Int J Adv Manuf Technol 95:3823–3837. https://doi.org/10.1007/s00170-017-1446-z

Figures

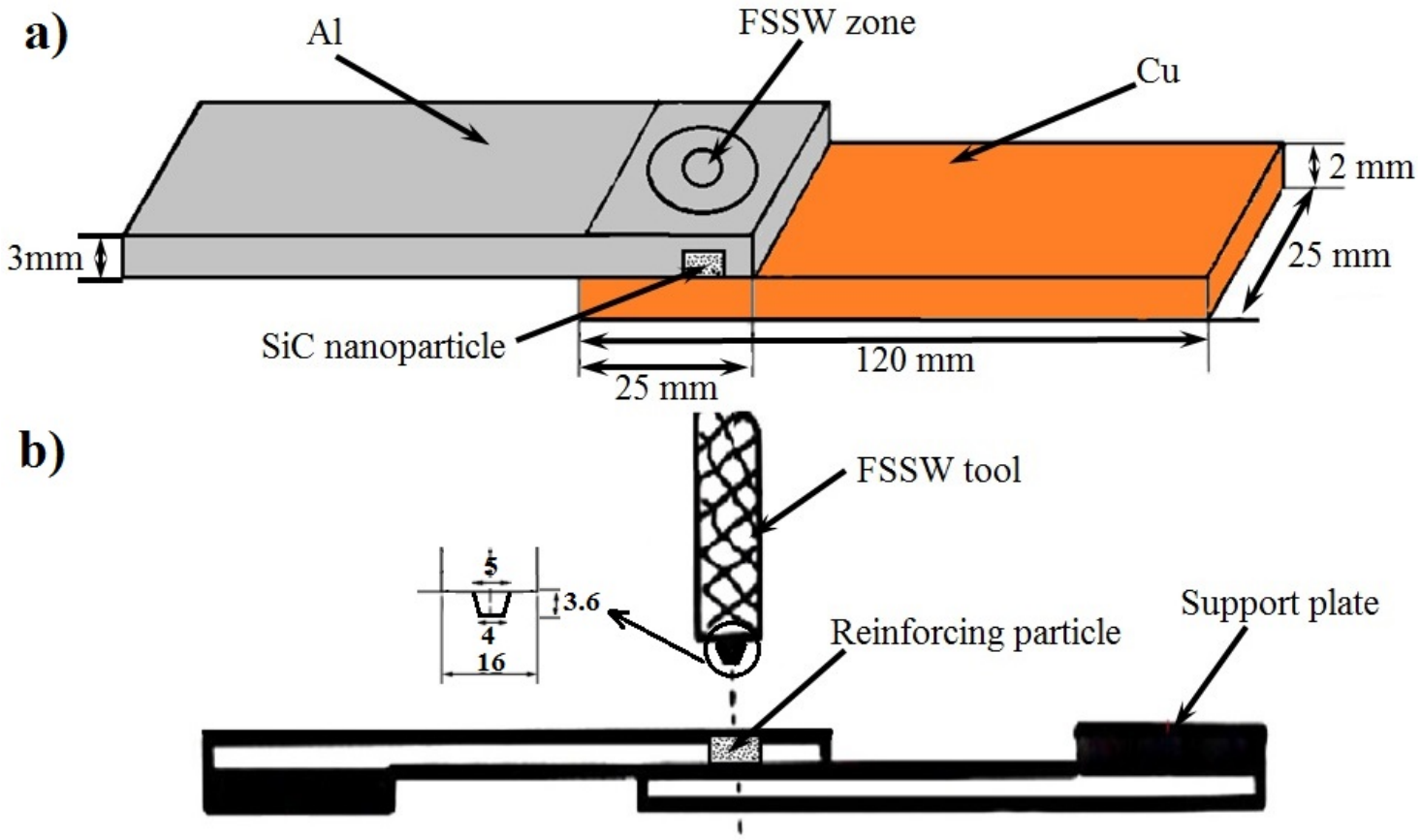

Figure 1

a) Schematic of FSSW process assembly, b) Dimensions of joining tool and SiC nanoparticle location (unit: mm)

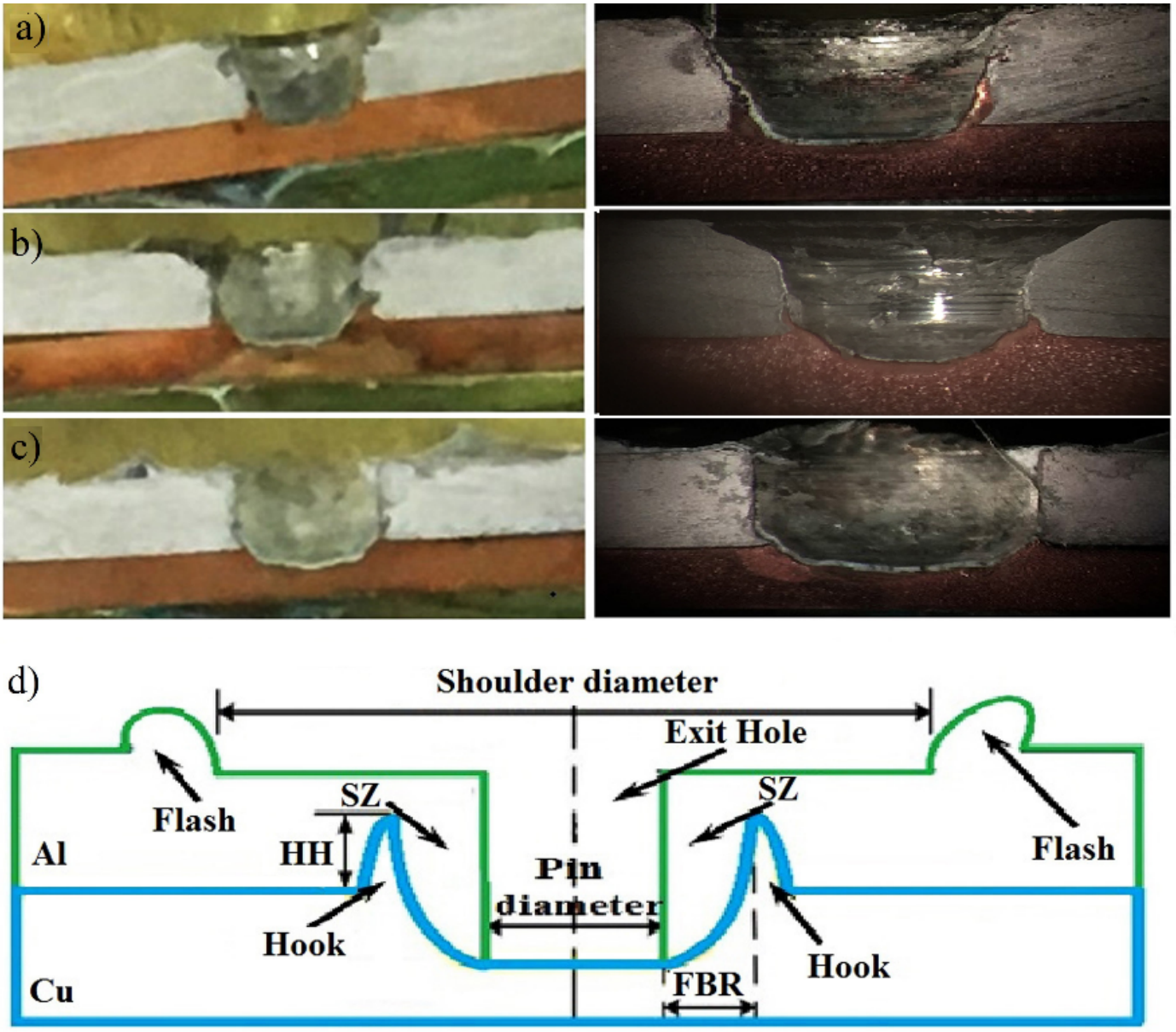

Figure 2

Impact of rotational speed and dwell time on macroscopic evolution of the weld zone (a) 1300 rpm, 2 s; (b) 1600 rpm, 2 s; (c) 1900 rpm, 2 s; (d) schematic of geometric parameters of the weld.

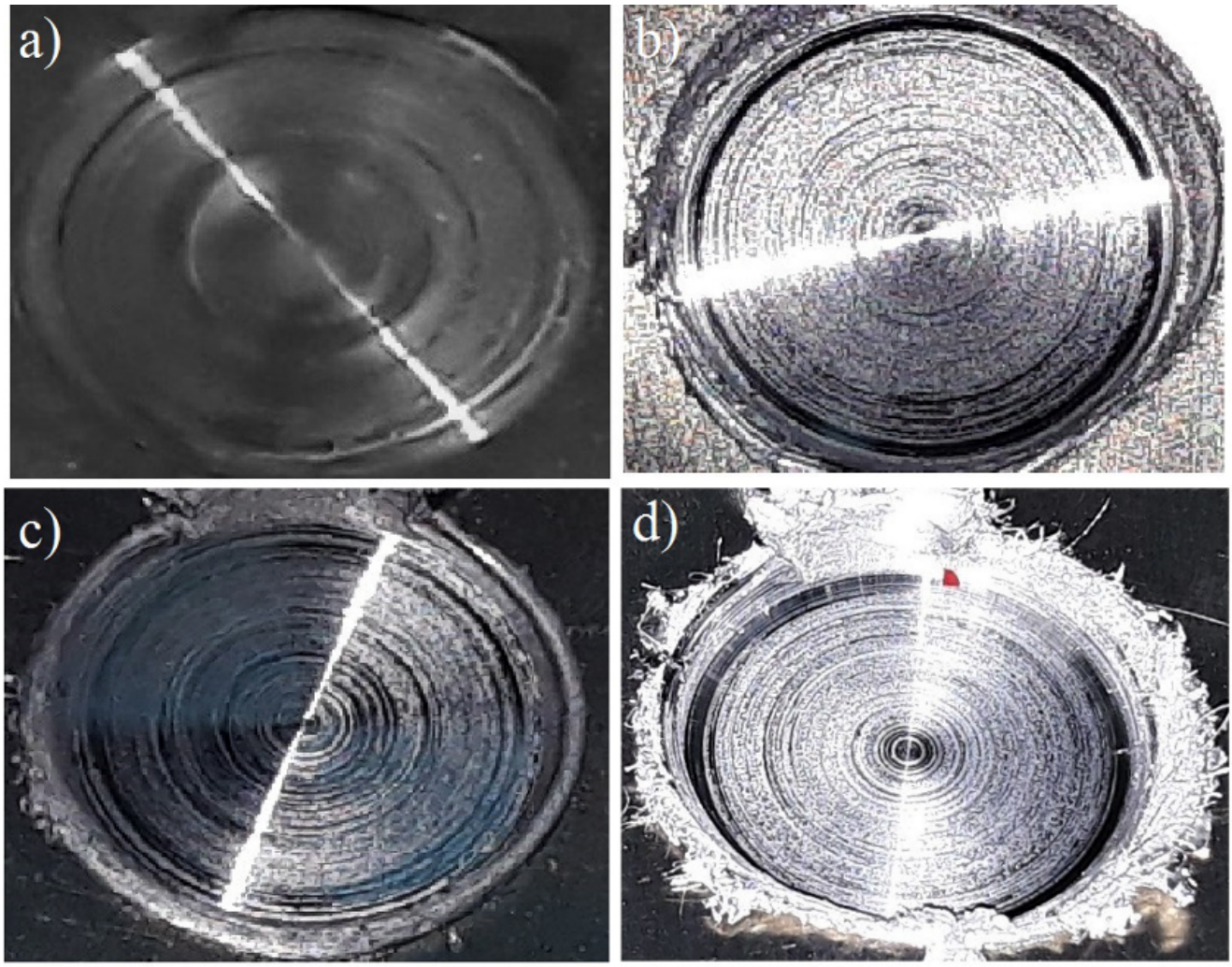

Figure 3

The top surface of the weld joint under different welding conditions: a) 1300 rpm, 2 s, b) 1300 rpm, 6 s, c) 1900 rpm, 2s, and d) 1900 rpm, 6s.

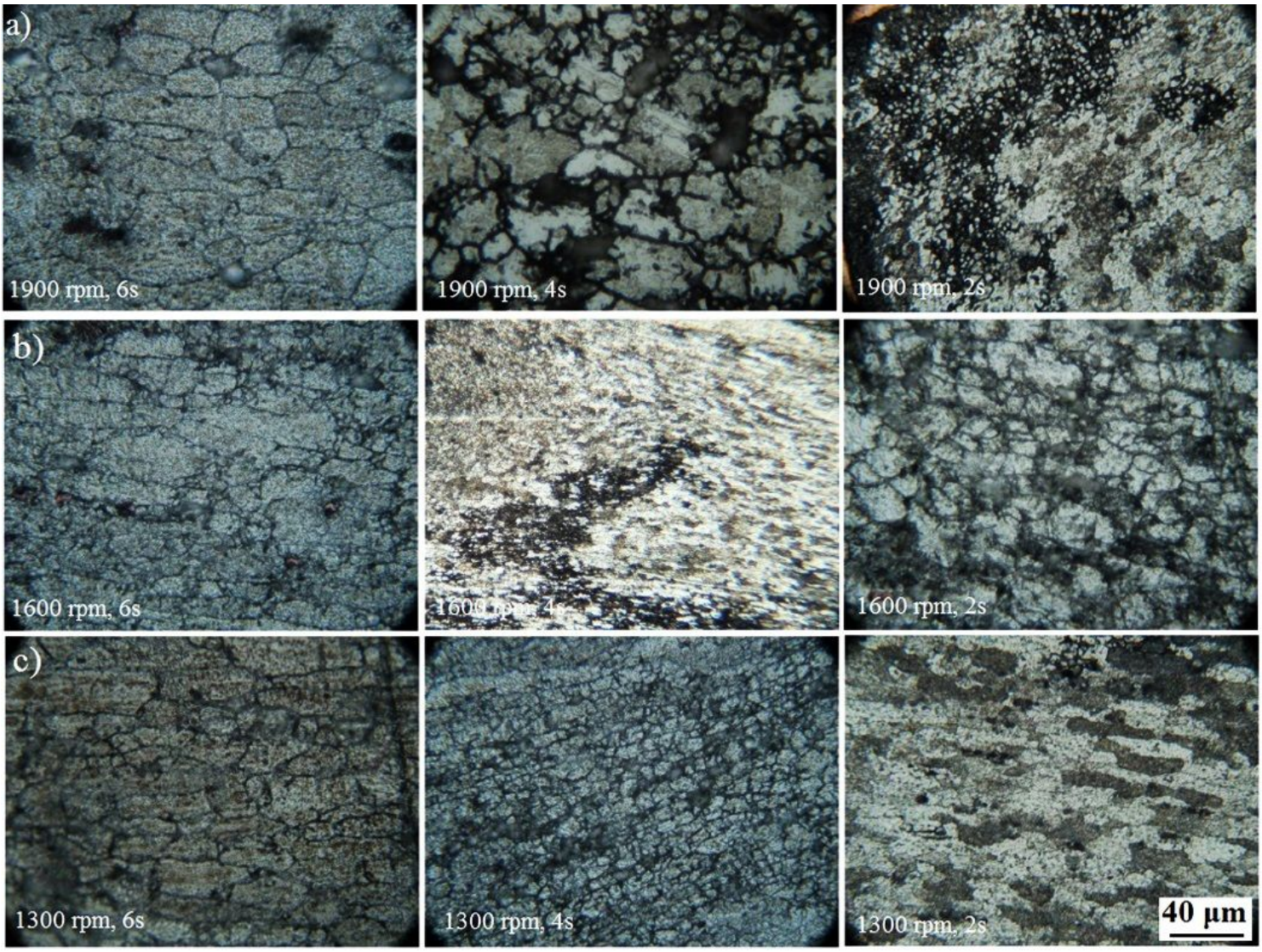

Figure 4

Microstructure evolution of the stir zone of Al side in FSSW of Al-Cu dissimilar alloys under different rotational speeds and dwelling time.

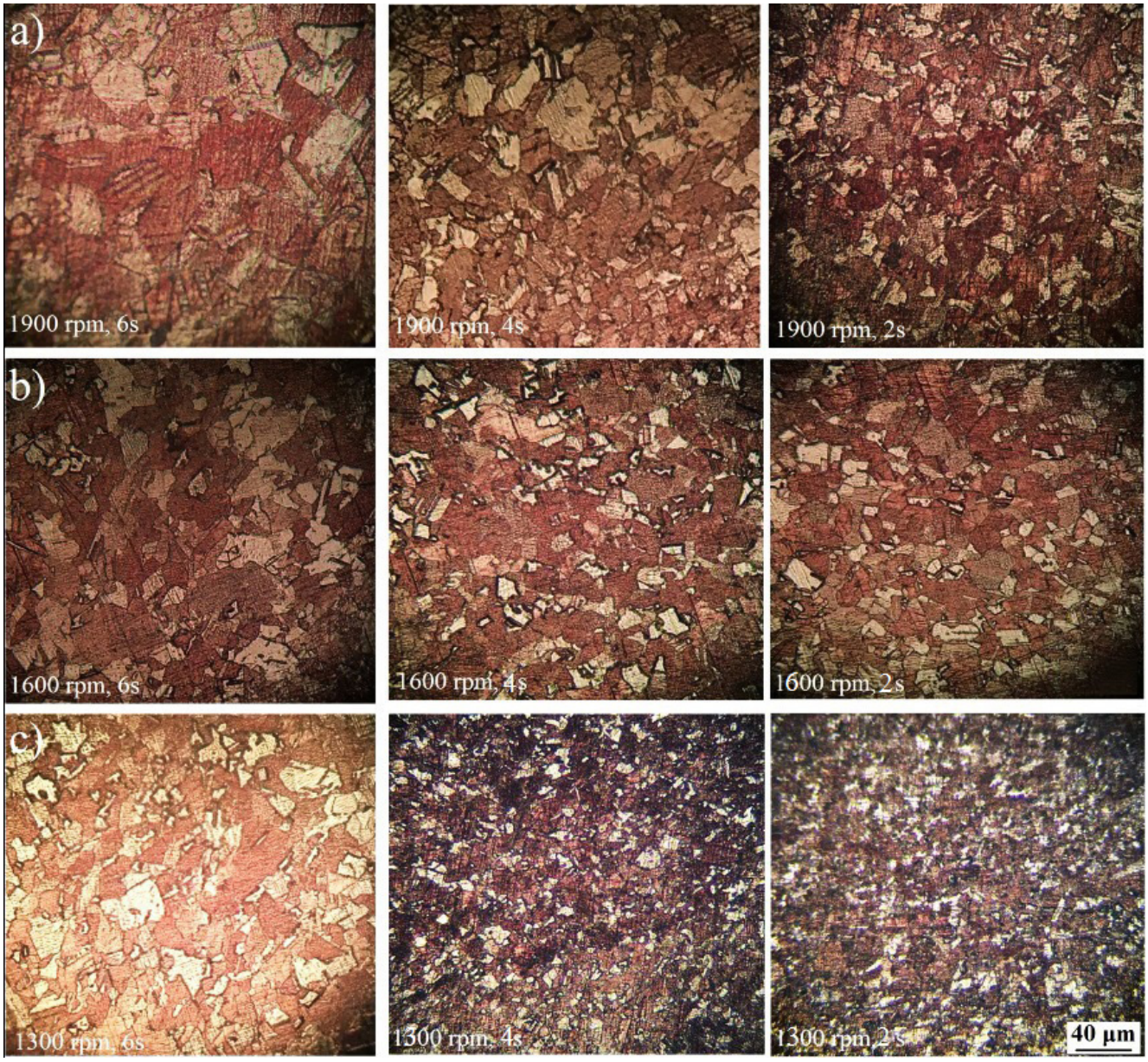

Figure 5

Microstructure evolution of the stir zone of Cu side in FSSW of Al-Cu dissimilar alloys under different rotational speeds and dwelling time.

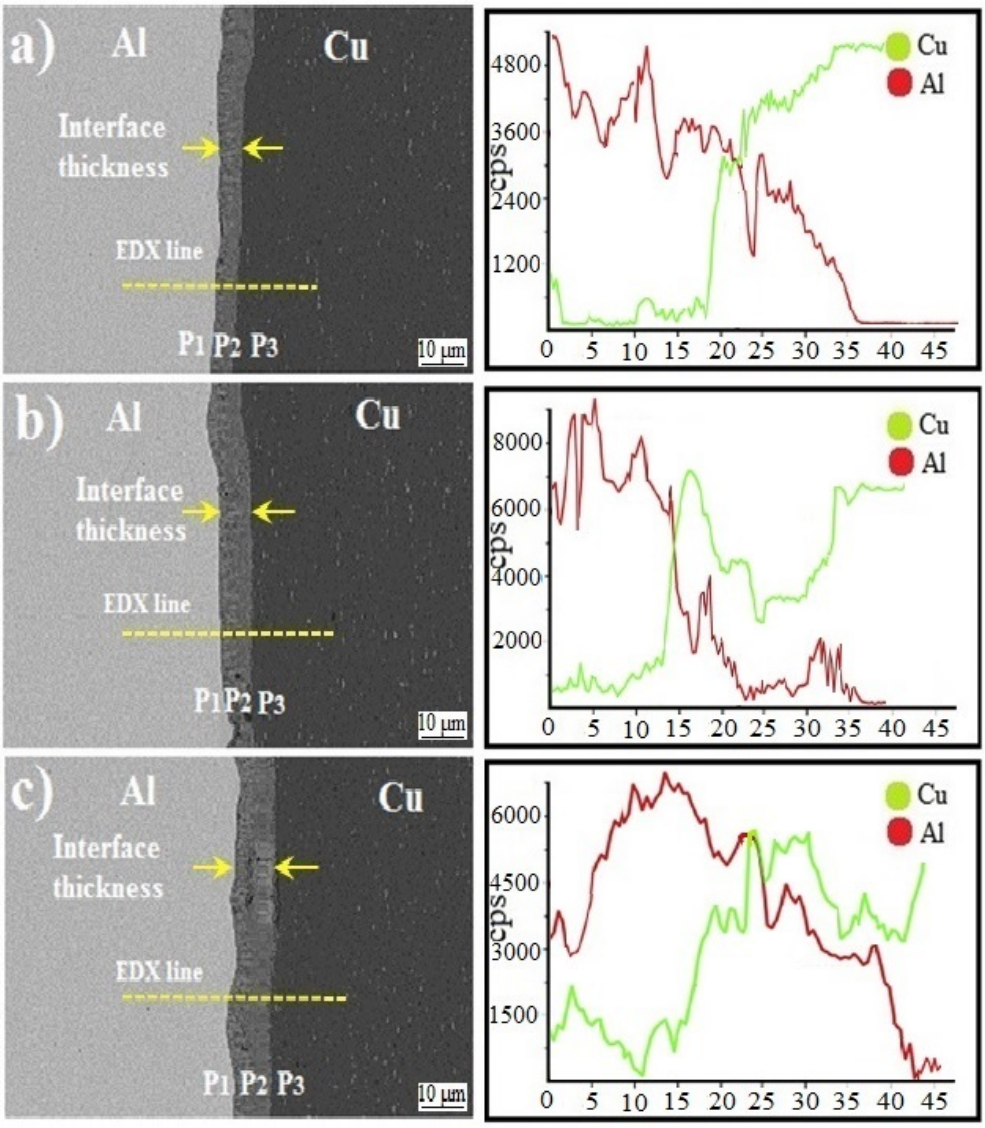

Figure 6

SEM analysis of the IMCs and EDX line scan data across the aluminum-copper weld interface at a) 1300 rpm, 2 s, b) 1300 rpm, 4 s, and c) 1300 rpm, 6s.

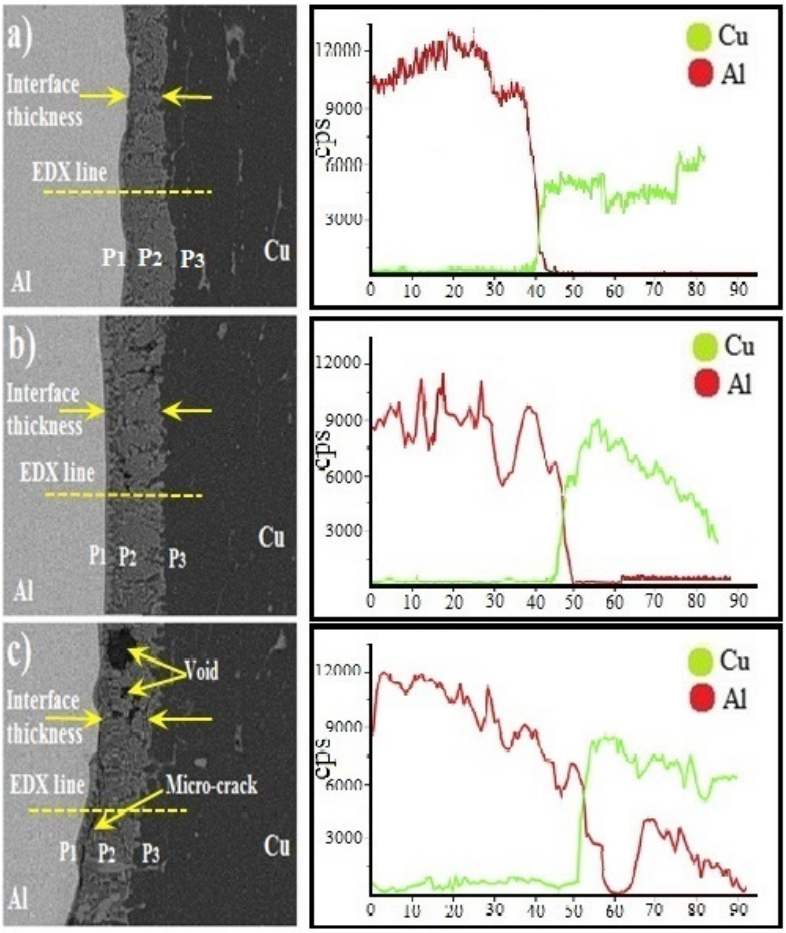

Figure 7

SEM analysis of the IMCs and EDX line scan data across the aluminum-copper weld interface at a) 1600 rpm, 2 s, b) 1600 rpm, 4 s, and c) 1600 rpm, 6s.

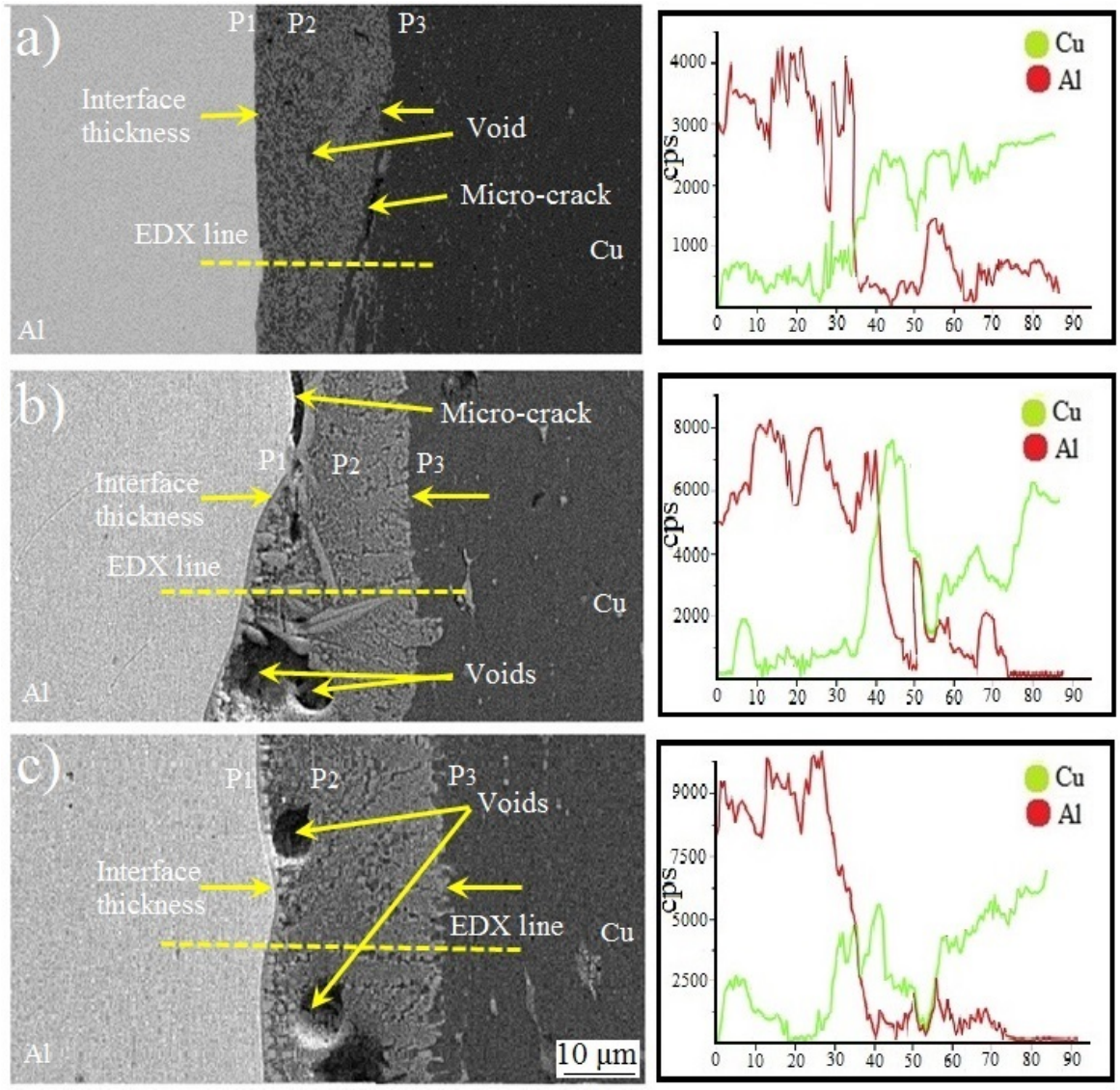

Figure 8

SEM analysis of the IMCs and EDX line scan data across the aluminum-copper weld interface at a) 1900 rpm, 2 s, b) 1900 rpm, 4 s, and c) 1900 rpm, 6s.

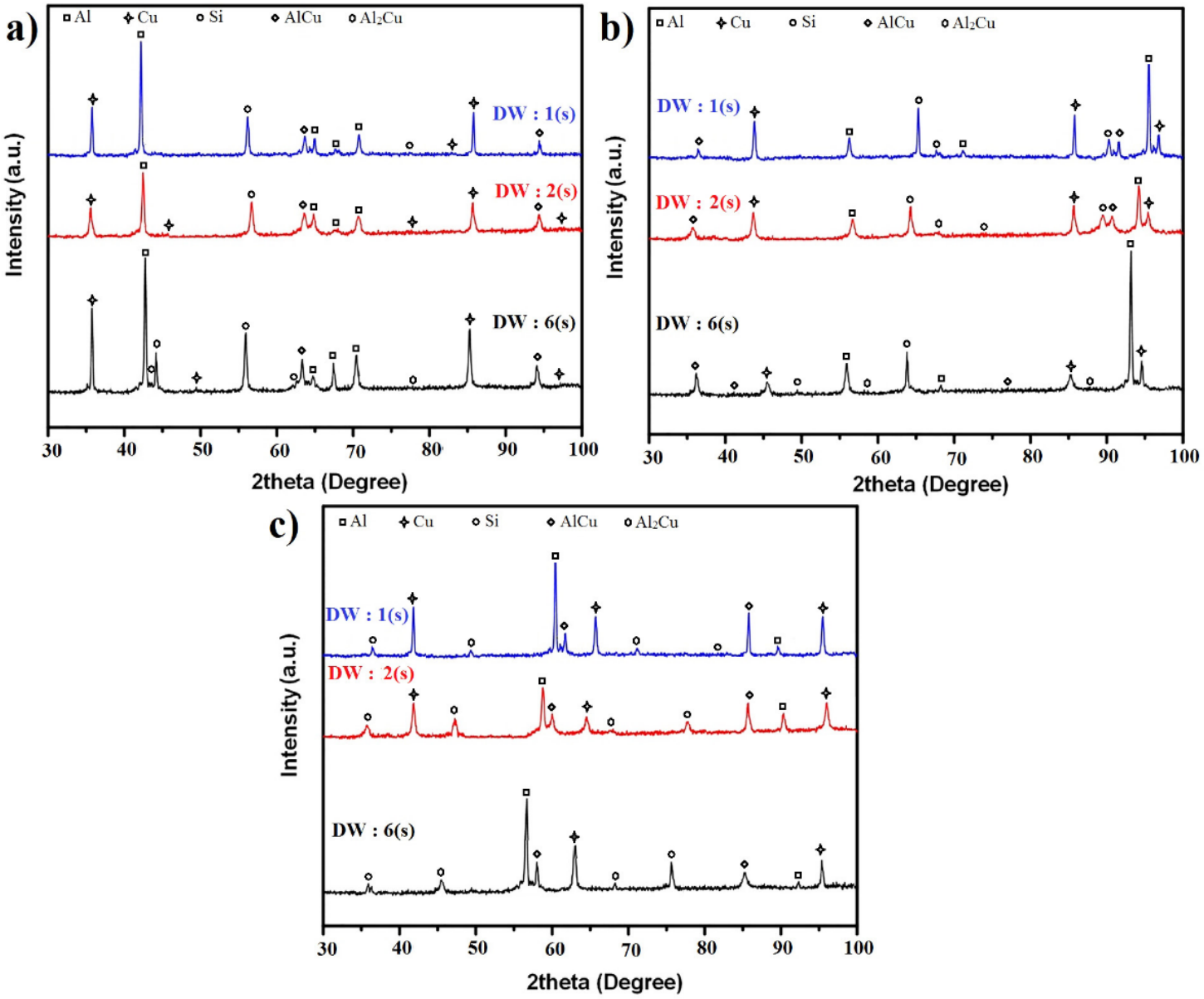

Figure 9

The XRD analysis outcomes from the cross-section of the relevant weld samples: a) 1300 rpm, b) 1600 rpm, and c) 1900 rpm.

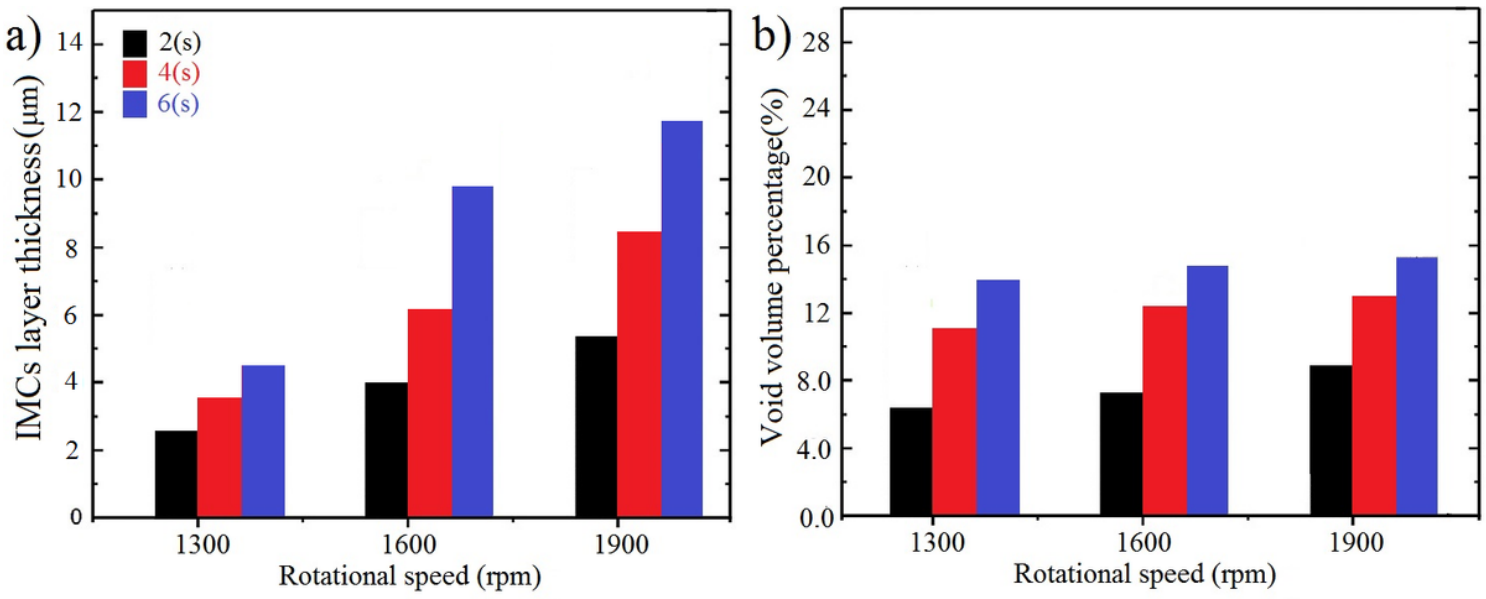

Figure 10

a) The thickness of IMC layers and b) void volume percentage under different welding conditions.

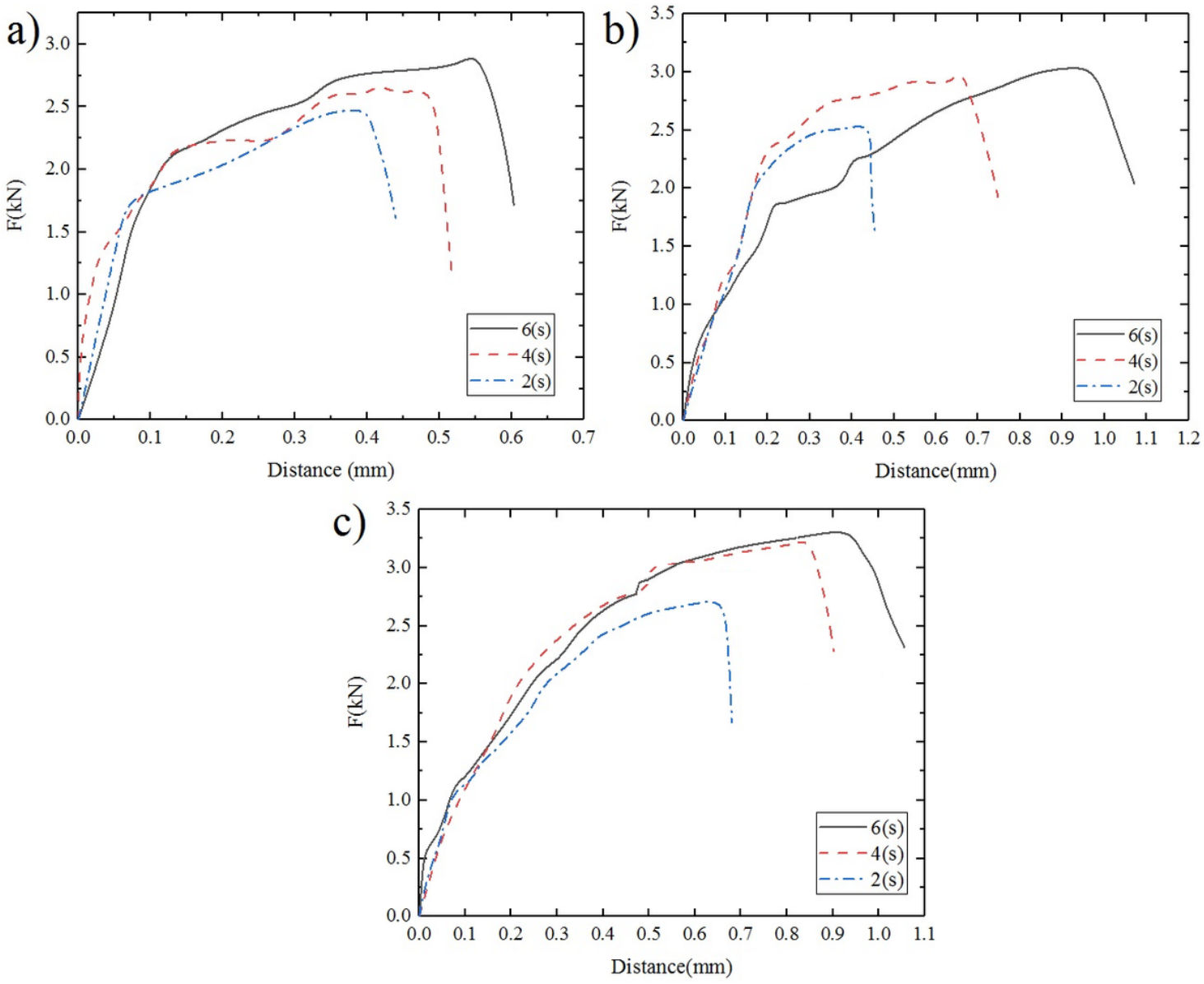

Figure 11

The tensile shear test of weld zone under different rotational speeds and dwell time. A) 1300 rpm, b) 1600 rpm, and c) 1900 rpm.

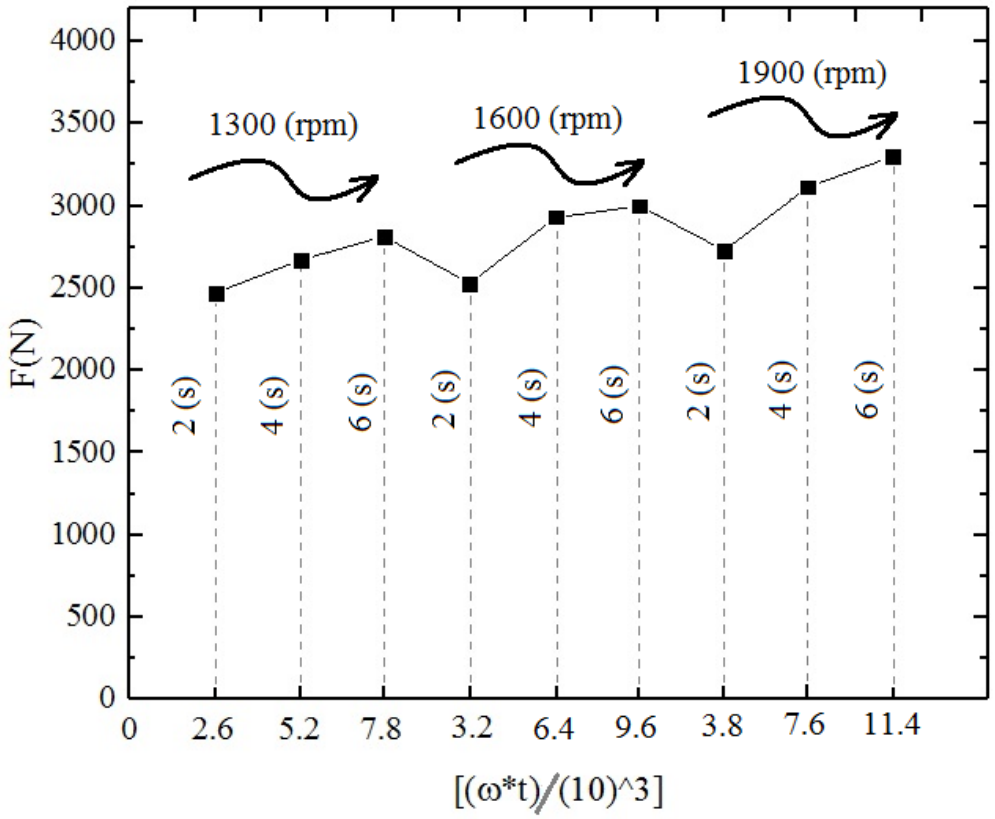

Figure 12

Relationship between input heat and tensile strength failure load.